Available online at www.sciencedirect.com
ScienceDirect
International Journal of Thermal Sciences 46 (2007) 235–244
International Journal of Thermal Sciences
www.elsevier.com/locate/ijts

Computation of the time-averaged temperature fields and energy fluxes in a thermally isolated thermoacoustic stack at low acoustic Mach numbers

A. Piccolo [a,*], G. Pistone [b]

[a] *Department of Civil Engineering, University of Messina, Contrada di Dio – 98166 S. Agata (Messina), Italy*
[b] *Department of Matter Physics and Advanced Physical Technologies, University of Messina, Contrada Papardo, Salita Sperone, 31-98166 S. Agata (Messina), Italy*

Received 31 May 2005; received in revised form 13 March 2006; accepted 13 June 2006

Available online 13 July 2006

Abstract

A simplified calculus model to investigate on the transverse heat transport near the edges of a thermally isolated thermoacoustic stack in the low acoustic Mach number regime is presented. The proposed methodology relies on the well-known results of the classical linear thermoacoustic theory which are implemented into an energy balance calculus-scheme through a finite difference technique. Details of the time-averaged temperature and heat flux density distributions along a pore cross-section of the stack are given. It is shown that a net heat exchange between the fluid and the solid walls takes place only near the edges of the stack plates, at distances from the ends not exceeding the peak-to-peak particle displacement amplitude. The structure of the mean temperature field within a stack plate is also investigated; this last results not uniform near its terminations giving rise to a smaller temperature difference between the plate extremities than that predicted by the standard linear theory. This result, when compared with experimental measurements available in literature, suggests that thermal effects localized at the stack edges may play an important role as sources of the deviations found between linear theory predictions and experiments at low and moderate Mach numbers.

Keywords: Thermoacoustics; Refrigerators; Heat; Sound; Finite differences

1. Introduction

Nowadays the thermoacoustic technology has the potential to play a major role in the development of more efficient energy conversion/generation systems sustainable in terms of costs, fuel resource availability and environmental acceptability. These potentialities derive from some inherent benefits thermoacoustic engines exhibit compared to their traditional counterparts (internal combustion engine, steam turbine, vapor compression refrigerator, etc.) and that make them very attractive for use in a variety of commercial and industrial applications. A thermoacoustic engine operates using non-polluting working fluids, has very few (often zero) moving mechanical parts, can utilize proportional control to adjust to shifting temperature/heat-loads and is made by traditional low-cost materials consisting basically of the following four components (see Fig. 1):

(1) a gas filled plane-wave resonator;
(2) an electro-acoustic transducer (acoustic driver);
(3) a porous solid medium (regenerator/stack);
(4) a couple of heat exchangers facing both ends of the stack.

The principles of thermoacoustic heat transport are exhaustively summarized, by the framework of the linear thermoacoustic theory, in Swift's tutorial article [1].

In its most simple and widely studied arrangement, the stack consists of an assembly of thin parallel plates aligned in the direction x of the particle acoustic oscillation (axial or longitudinal direction) and spaced by no more than few thermal penetration depths, δ_κ, the distance through which heat can diffuse in an acoustic cycle. This element, defined as the "heart" of the engine, gives place to the desired heat/sound energy conversion, the so-called "thermoacoustic effect". Detailed outlines

* Corresponding author. Tel.: +39 090 3977311; fax: +39 090 3977480.
E-mail address: apiccolo@unime.it (A. Piccolo).

1290-0729/$ – see front matter
doi:10.1016/j.ijthermalsci.2006.06.004

Nomenclature

a	speed of sound	$\mathrm{m\,s^{-1}}$
A	cross-sectional area	$\mathrm{m^2}$
c_P	isobaric specific heat of the gas	$\mathrm{J\,kg^{-1}\,K^{-1}}$
c_s	specific heat of the plate material	$\mathrm{J\,kg^{-1}\,K^{-1}}$
$\dot{\mathbf{e}}$	time-averaged energy flux density	$\mathrm{W\,m^{-2}}$
f	frequency	Hz
f_v	spatially averaged thermoviscous function	
h	thermoviscous function	
$\dot{h}$	time-averaged enthalpy flux density	$\mathrm{W\,m^{-2}}$
$\dot{H}$	total enthalpy flux in half a channel	W
i	imaginary unit	
k	wave number	$\mathrm{m^{-1}}$
K	thermal conductivity	$\mathrm{W\,m^{-1}\,K^{-1}}$
l	half of the plate thickness	m
L_s	stack length	m
M	Mach number	
$\mathbf{n}$	unit vector	
P	pressure	Pa
Pr	Prandtl number	
$\dot{q}$	time-averaged heat flux density	$\mathrm{W\,m^{-2}}$
S	surface	$\mathrm{m^2}$
t	time	s
T	temperature	K
∇T_E	longitudinal temperature gradient for which $\dot{h}_x = 0$	$\mathrm{K\,m^{-1}}$
u	x-component of the acoustic particle velocity	$\mathrm{m\,s^{-1}}$
U	volume flow rate	$\mathrm{m^3\,s^{-1}}$
x	axial coordinate (direction)	m
	acoustic particle displacement	m
x_s	mean distance of the stack from the centre of the resonator	m
y	transverse coordinate (direction) perpendicular to the plate surface	m
y_0	half distance between two plates	m
z	transverse coordinate (direction) direction perpendicular to the x–y plane	m

Greek symbols

δ	penetration depth	m
Δx	computation mesh size along the x direction	m
Δy	computation mesh size along the y direction	m
ΔT	temperature difference between the plate extremities	K
λ	wavelength of the sound wave	m
ξ	generic acoustic variable	
ρ	density of the gas	$\mathrm{kg\ m^{-3}}$
ω	angular frequency of the sound wave	$\mathrm{rad\,s^{-1}}$
Ω	blockage ratio	

Subscripts

0	evaluated at the mean stack position
1	first order acoustic variable
A	acoustic amplitude at a pressure antinode
E	end
m	mean, time averaged
max	maximum value
P	isobaric
res	resonator
s	solid, stack
x	longitudinal
y	transversal
α	term “alpha” of the enthalpy flux
β	term “beta” of the enthalpy flux
κ	thermal
ν	viscous

Superscripts

i	nodal point index
j	nodal point index

of the criteria generally applied to optimize the stack performance can be found in [2,3]. Two heat exchangers (“hot” and “cold” exchangers), placed in close proximity of both ends of the stack, absolve to the task of either supplying or removing heat from its edges thus enabling heat transfer with the external world.

The coupling between the stack and the heat exchangers is actually recognized as a fundamental problem in thermoacoustic engines design and a major challenge for the future improvement of the overall engine’s performances. Optimal design of thermoacoustic heat exchangers depends on the understanding of the thermo-fluid dynamic processes controlling the heat transfer between the sound wave and the heat exchangers at the heat exchanger–stack junctions. The starting point for the solution of this problem is the analysis of the structure of the time-averaged temperature, energy and flow fields near the pore ends of the stack.

The conventional linear thermoacoustic theory [1], precludes treatments of the gas–solid heat transfer mechanisms at the plate edges of the stack. Its formulation, in fact, is based on the simplifying assumption that the time-averaged temperature of the gas, T_m, is constant over a cross section of a stack channel and the same as that of the adjacent solid surface, T_{sm}. The only dependence allowed for both gas and plates time-averaged temperatures is the one along the axial direction, so precluding any net heat exchange between them. This hypothesis evidently fails in proximity of the stack ends (or in the heat exchangers) where net gas–solid heat transfer takes place as a result of non-zero temperature gradients along the direction y normal to the plate surfaces (transverse direction). Swift, for example, analyzing the performance of a thermoacoustic prime mover [4], measured significant time-averaged temperature differences between the gas and cold heat-exchanger fins; at low Mach numbers ($M < 4\%$), these differences were observed to

increase proportional to the acoustic pressure amplitude while at higher M values the growth became faster. Other experimental evidences of non-constant temperature gradient in the stack are given in [5–7].

Considerable theoretical research focused on the study of the temperature and heat flux distributions inside a gas channel of thermally isolated parallel-plate stacks much shorter in length than the acoustic wavelength. These simplified structures (for which no heat can be exchanged either transversely or axially through the ends with the surroundings) lead to a simpler mathematics compared to other stack geometries [8–10], still retaining most of the physics of the problem. Numerical methods were applied by Cao et al. [11] who integrated the compressible two-dimensional Navier–Stokes equations to test the effect of plate spacing and acoustic pressure on the gas–solid heat exchange area. Worlikar et al. [12,13] used a low Mach number model to analyze the steady-state temperature stratification in short stacks. Ishikawa and Mee [14] also considered in their computations plate lengths short compared to the particle displacement length. Recent developments can be found in the work of Besnoin and Knio [15] and in that of Marx and Blanc-Bennon [16] where the coupling between the stack and the heat exchangers was investigated. Analytical methods were applied by Mozurkewich [17,18], Gopinath et al. [19], Gusev et al. [20,21] and Waxler [22]. Yet some aspects are still not fully understood, even at low and moderate acoustic Mach numbers (less than a few percent), such as the relative incidence of non-linear acoustic effects, turbulence, thermal effects and other local physical processes on the disagreement between standard linear theory predictions and experiments [23,24].

To delve into the above phenomena, a simplified numerical model for describing time-average transverse heat transfer near the edges of a thermally isolated thermoacoustic stack at low Mach numbers is presented in this paper. The proposed methodology, inspired by the approach proposed in [17], relies on the well-known results of the classical linear thermoacoustic theory, in the "short stack" approximation formulation, for the main energy-transport variables. They are implemented into a simple energy balance calculus-scheme through a finite difference technique. The basic assumption are (a) that the solutions of the classical linear theory for the amplitude of the acoustic temperature oscillation, T_1, and associated enthalpy flux equation, are approximately valid near the pore ends and (b) that thermal conduction is the unique mechanism of heat transport along the transverse y direction at any distance from the plate surfaces. The numerical results concerning the structure of the two-dimensional temperature and energy-flux distributions both in a solid plate and in a gas channel of the stack are presented. A comparison with the findings of numerical calculations and experimental measurements to be found in literature is also proposed. Furthermore, the limitations of the model are explained.

2. Formulation

For pate lengths sufficiently greater than the particle displacement length, however respecting the short stack approximation (see below), the solutions of the standard linear theory for the energy-transport variables should hold precisely in the central regions of the stack, where end effects are negligible. We show as, in the cases in which these solution may be retained (sufficiently) accurate also near the pore terminations, they can be easily implemented in a simple calculus-scheme to describe time-average transverse heat transfer at the stack edges. The proposed methodology involves only energy balance and boundary conditions specific to the case-study.

To start with the explicit formulation of the calculus model we observe that for problems characterized by a periodic time dependence (like thermoacoustics), the time-averaged law of conservation of energy for a compressible viscous fluid is expressed by the equation [25]:

$$\nabla \cdot \dot{\mathbf{e}} = 0 \tag{1}$$

Integrating this equation over a volume element bounded by a closed surface S and applying the divergence theorem gives us

$$\oint_S \dot{\mathbf{e}} \cdot \mathbf{n}\, \mathrm{d}S = 0 \tag{2}$$

where $\mathbf{n}$ is the unit vector directed along the normal to the surface element $\mathrm{d}S$. Eqs. (1) and (2) state equivalently that the time-averaged energy flux density, $\dot{\mathbf{e}}$, is a conserved quantity. In particular, Eq. (2) can be conveniently applied to whatever sub-region traced in the gas to impose local energy balance. To accomplish this, a finite difference technique may be used, where the quantitative results of standard linear theory can be considered for the components of the time-averaged energy flux density along the directions of interest.

The thermoacoustic equation for the hydrodynamic energy flux density along the x direction is derived in the simplified case of a parallel-plate stack. The ratio of the plate spacing (and of the plate thickness) to the width in the transverse direction is taken to be very small (as in real cases) thus the energy flow along the z direction (perpendicular to the x–y plane) is negligible and the problem can be regarded as two-dimensional.

The conventional complex notation is adopted for the time-dependent variables

$$\xi(t) = \xi_m + \mathrm{Re}\left\{\xi_1 e^{i\omega t}\right\} \tag{3}$$

where t is the time, i the imaginary unit, Re{ } signifies the real part and where ξ_1 is the first-order complex amplitude of the variable ξ fluctuating with angular frequency ω about its mean value ξ_m.

The time-averaged hydrodynamic energy flow in the gas along the longitudinal direction x is the same as the time-averaged hydrodynamic enthalpy flow $\dot{h}_x$ [1]:

$$\dot{h}_x = \rho_m c_P \frac{\omega}{2\pi} \int_0^{2\pi/\omega} T(t)u(t)\, \mathrm{d}t = \frac{1}{2}\rho_m c_P\, \mathrm{Re}\{T_1 \tilde{u}_1\} \tag{4}$$

where ρ_m is the mean density of the gas, c_P is the isobaric specific heat of the gas, T is the temperature, u is the x-component of the acoustic particle velocity, tilde indicates complex conjugation and having assumed the fluid obeys to the ideal gas

equation of state. To evaluate this quantity, explicit expressions for the first-order complex amplitudes T_1 and u_1 inside the stack are required. If the specific heat of the plate material, c_s, is notably greater than c_P, it results [1,26]:

$$T_1 = \frac{1}{\rho_m c_P}(1-h_\kappa)P_1 - \frac{1}{\rho_m \omega^2}\frac{\mathrm{d}P_1}{\mathrm{d}x}\frac{\mathrm{d}T_m}{\mathrm{d}x}\left[\frac{(1-h_\kappa)-Pr(1-h_\nu)}{(1-Pr)}\right] \quad (5)$$

$$u_1 = \frac{i}{\omega\rho_m}\frac{\mathrm{d}P_1}{\mathrm{d}x}(1-h_\nu) \quad (6)$$

where

$$h_\kappa = \frac{\cosh[(1+i)y/\delta_\kappa]}{\cosh[(1+i)y_0/\delta_\kappa]}, \qquad h_\nu = \frac{\cosh[(1+i)y/\delta_\nu]}{\cosh[(1+i)y_0/\delta_\nu]} \quad (7)$$

P_1 being the local amplitude of the dynamic pressure, Pr the Prandtl number, y_0 half distance between two plates, δ_ν the viscous penetration depth and where $y=0$ is in the center of the fluid gap.

A simple expression for the pressure derivative $\mathrm{d}P_1/\mathrm{d}x$ can be derived (see [27]) if the stack satisfies the "short stack approximation" which can be synthesized as follows:

(a) the reduced acoustic wavelength, $\lambda/2\pi$, is much larger than the stack length, L_s. This implies that the stack may be retained to be acoustically non-intrusive so that pressure and velocity may be approximated at the entrance of the stack with the equations given by lossless acoustics that, for a half-wavelength resonator, are:

$$P_1 = P_A \sin kx_s = P_0 \quad (8)$$

$$u_1 = i\frac{P_A}{\rho_m a}\cos kx_s = iu_0 \quad (9)$$

P_A being the amplitude of the dynamic pressure at a pressure antinode, k the wave number ($k=2\pi/\lambda$), a the sound velocity and x_s the mean stack location calculated as the distance of the stack from the centre of the resonator (in the short stack approximation the stack entrance location can merge its mean location without appreciable errors in P_1 and u_1).

(b) the temperature difference across the stack is much less than the mean stack temperature so that the dependence of the thermophysical parameters of the gas on the temperature, and thus on x, can be neglected inside the stack.

Using Eq. (9), we can write for the volume flow rate at the entrance of the stack

$$U_1 = A_{\mathrm{res}}u_1 = iA_{\mathrm{res}}u_0 \quad (10)$$

A_{res} being the cross sectional area of the resonator. Eq. (6) can be integrated over the cross section of a pore to obtain U_1 within the stack

$$U_1 = \frac{A_s}{y_0}\int_0^{y_0} u_1(y)\,\mathrm{d}y = \frac{iA_s}{\omega\rho_m}\frac{\mathrm{d}P_1}{\mathrm{d}x}(1-f_\nu) \quad (11)$$

where

$$f_\nu = \frac{\tanh[(1+i)y_0/\delta_\nu]}{[(1+i)y_0/\delta_\nu]} \quad (12)$$

and where A_s is the cross sectional area of the stack open to gas flow. By imposing now continuity of volume flow rate at the entrance of the stack, Eqs. (10) and (11) can be equated to find $\mathrm{d}P_1/\mathrm{d}x$ just inside and, by approximation, along the stack

$$\frac{\mathrm{d}P_1}{\mathrm{d}x} = \frac{u_0}{\Omega}\frac{\rho_m\omega}{(1-f_\nu)} \quad (13)$$

where the blockage ratio $\Omega = A_s/A_{\mathrm{res}} = 1/(1+l/y_0)$ describes the porosity of the stack.

Substituting now Eqs. (8) and (13) into Eqs. (5) and (6) and these last in Eq. (4), the following expression is found, at second order in the acoustic oscillation amplitude, for $\dot{h}_x$:

$$\dot{h}_x = \frac{1}{2\Omega}\mathrm{Im}\left[\frac{(1-\tilde{h}_\nu)(1-h_\kappa)}{(1-\tilde{f}_\nu)}\right]P_0u_0 - \frac{c_P\rho_m}{2\omega\Omega^2(1-Pr)}\frac{\mathrm{d}T_m}{\mathrm{d}x}\mathrm{Im}\left[\frac{(1-h_\kappa)(1-\tilde{h}_\nu)}{|1-f_\nu|^2}\right]u_0^2 \quad (14)$$

Note that for a given stack location (x_s) in the resonator, all quantities in this equation may be assumed independent of the axial coordinate x within the stack except T_m; quantities enclosed in square brackets, on the other hand, depend only on the y coordinate reflecting the transverse variation of u_1 and T_1. Eq. (14) is reasonably accurate in the central regions of the stack pore where the energy flux is expected to be strictly unidirectional (along x), the net heat transfer between fluid and plate being zero. At the pore ends, however, where the mean temperature field becomes y-dependent, its validity is questionable because it was derived from Eq. (5), which is solution of the heat transport equation involving a y-independent T_m. Application of Eq. (14) in regions near the pore ends constitutes therefore an approximation which is expected to be valid as long as significant transverse temperature gradients do not develop within the stack, namely, at low acoustic Mach numbers. The same assumption, on the other hand, has been successfully applied in [17] to derive a differential equation for the time-averaged gas temperature. From a analytical point of view, this approximation lets in Eq. (14) T_m and its derivative $\mathrm{d}T_m/\mathrm{d}x$ to be both x and y dependent. Thus, in the following we rewrite Eq. (14) in the form

$$\dot{h}_x(x,y) = \dot{h}_\alpha(y) - \frac{\partial T_m(x,y)}{\partial x}\dot{h}_\beta(y) \quad (15)$$

where

$$\dot{h}_\alpha(y) = \frac{1}{2\Omega}\mathrm{Im}\left[\frac{(1-\tilde{h}_\nu)(1-h_\kappa)}{(1-\tilde{f}_\nu)}\right]P_0u_0 \quad (16)$$

and

$$\dot{h}_\beta(y) = \frac{c_P\rho_m}{2\omega\Omega^2(1-Pr)}\mathrm{Im}\left[\frac{(1-h_\kappa)(1-\tilde{h}_\nu)}{|1-f_\nu|^2}\right]u_0^2 \quad (17)$$

are both real and positive quantities.

The energy flux density along the axial direction comprises also the diffusive term $-K\partial T_m/\partial x$ (K being the thermal conductivity of the gas). This contribution is generally considered to be negligible in comparison to the hydrodynamic-one [17] and therefore will be here neglected.

On the opposite hand, the transverse component of the energy flux density contains, by hypothesis, only the diffusive term

$$\dot{q}_y = -K\frac{\partial T_m}{\partial y} \tag{18}$$

where $\dot{q}_y$ is the time-averaged heat flux density along the transverse direction. This assumption is certainly valid near the plate surface where the fluid is at rest. Within the linear theory, however, it may be considered reasonable also in regions far from the plate surface. Being in fact $\partial/\partial x \sim 1/\lambda$ and $\partial/\partial y \sim 1/\delta_\kappa$, the velocity in the y direction is of order δ_κ/λ smaller than u_1. This entails, as verified in [28], that the hydrodynamic heat fluxes along the y direction are very small compared to the diffusive-ones.

Since a x-dependent derivative $\partial T_m/\partial x$, and thus a x-variable $\dot{h}_x$ along the stack, implies net heat deposition into and/or extraction out of the solid plates, Eqs. (15) and (18) must be related to the analogues in the solid walls. If K_s is the thermal conductivity of the plate material, the time-averaged heat flux densities along the x and y directions are simply

$$\dot{q}_x = -K_s\frac{\partial T_{sm}}{\partial x}, \qquad \dot{q}_y = -K_s\frac{\partial T_{sm}}{\partial y} \tag{19}$$

after taking into account that thermal conduction is the unique mechanism of energy transport inside the stack plates and that, being by hypothesis $c_s \gg c_p$, the solid temperature oscillations are negligible.

3. Numerical model

The simulation model system is a thermally isolated stack of parallel plates, of length L_s located at position x_s in a half-wavelength gas filled resonator sustaining a standing acoustic wave as shown in Fig. 1 (excluding the heat-exchangers). As a stack is usually constituted by a set of identical plates, calculations were performed in a single channel of the stack, i.e. between a single pair of parallel plates. The simulation domain is further reduced by symmetry from half a gas duct to half a plate and is indicated in Fig. 2 by the light grey area together with the coordinate system used. The axis parallel to the plates is the x axis; $x = 0$ is chosen to be the beginning of the stack on the left. The y axis is perpendicular to the stack-plates; $y = 0$ is chosen to be the midpoint between the two adjacent plates.

The calculation of the steady-state two-dimensional time-averaged temperature distribution was performed using a finite difference methodology. To this end, the computational domain was subdivided using a rectangular grid. In the x direction the computation mesh size, Δx, was typically $0.0041L_s$ while in the y direction the computation mesh size, Δy, was typically $0.02y_0$. The set of finite-difference equations for the unknown quantities $T_m(x, y)$ and $T_{sm}(x, y)$ was then derived imposing energy balance at each nodal point of the computational grid making use of Eqs. (15) and (18) for the x and y components of the energy flux density in the gas and of Eqs. (19) for the analogues in the solid. Temperature spatial gradients were discretized using first order nodal temperature differences. As an

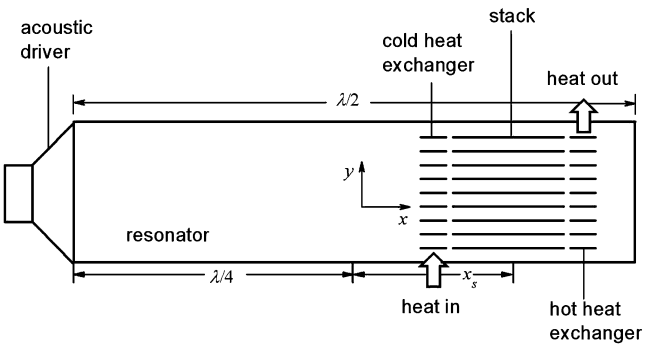

Fig. 1. Schematic illustration of a thermoacoustic refrigerator.

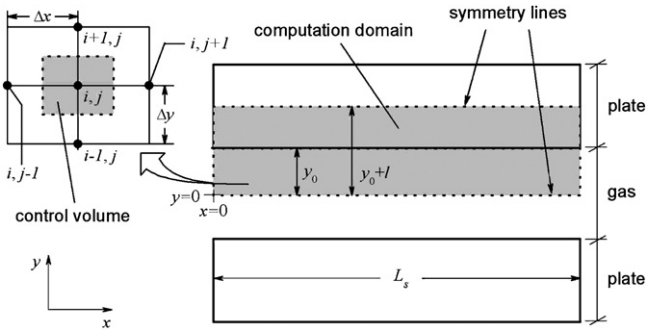

Fig. 2. Magnified region of two stack plates. The light grey areas indicate the computation domain and the control volume about a generic nodal point.

example, for a nodal point laying in the gas region of the simulation domain (see Fig. 2) the resulting equation is:

$$K\frac{\Delta x}{\Delta y}T_m^{i-1,j} + \dot{h}_\beta\frac{\Delta y}{\Delta x}T_m^{i,j-1} + \left(-2\dot{h}_\beta\frac{\Delta y}{\Delta x} - 2K\frac{\Delta x}{\Delta y}\right)T_m^{i,j} + \dot{h}_\beta\frac{\Delta y}{\Delta x}T_m^{i,j+1} + K\frac{\Delta x}{\Delta y}T_m^{i+1,j} = 0 \tag{20}$$

which is Eq. (2) applied to the control volume about node (i, j). Analogue equations yield for nodal points laying in the plate, while to derive the system-equations for nodal points laying on boundary lines, symmetry lines and on the gas-plate interface line, the following boundary conditions were imposed:

- nodal lines at $y = 0$ and $y = y_0 + l$ are symmetry lines so

$$\left(\frac{\partial T_m}{\partial y}\right)_{y=0} = 0, \qquad \left(\frac{\partial T_{sm}}{\partial y}\right)_{y=y_0+l} = 0 \tag{21}$$

- continuity conditions at the fluid–solid interface ($y = y_0$) entail that the time-averaged temperature of the gas corresponds to the plate temperature and that the energy flux leaving (or entering) the gas equals that entering (or leaving) the solid wall

$$T_m(y = y_0) = T_{sm}(y = y_0)$$
$$K\left(\frac{\partial T_m}{\partial y}\right)_{y=y_0} = K_S\left(\frac{\partial T_{sm}}{\partial y}\right)_{y=y_0} \tag{22}$$

- for a thermally isolated stack no heat may leave or enter the stack diffusively across the plates terminations ($y_0 \leqslant y \leqslant y_0 + l$)

$$\left(\frac{\partial T_{sm}}{\partial x}\right)_{x=0} = 0, \qquad \left(\frac{\partial T_{sm}}{\partial x}\right)_{x=L_s} = 0 \tag{23}$$

- for a thermally isolated stack no energy may leave or enter the stack hydrodynamically across the pore ends ($0 \leqslant y < y_0$)

$$\dot{h}_x(x=0) = 0, \qquad \dot{h}_x(x=L_s) = 0 \tag{24}$$

Note that the above condition was judged too strong by the author of [17] who, alternatively, suggested (and applied) the requirement that the axial temperature gradient should be uniform at the pore-end and approaches the constant value for which the integral of $\dot{h}_x$ over the section vanishes. Even if this weaker condition allows for recirculating energy fluxes at the pore terminations (both positive and negative energy fluxes crossing the end section can simultaneously exist being their sum zero), it introduces a discontinuity in the axial temperature gradient at the gas–solid interface; as here the fluid comes to rest and thermal conduction becomes the predominant mechanism of energy transport, it could expected that, at approaching the fluid–solid interface $\partial T_m/\partial x$ tends to vanish, so matching the zero gradient which is found at the plate terminations according to (22) and (23). As it will be shown in Section 4, this is indeed the case if conditions (24) are applied, even if this does not constitute a proof for preferring these conditions respect to the weaker-ones.

The elements of the coefficient matrix associated to the resultant system of linear algebraic equations were calculated using a code developed by the authors in FORTRAN-77 language and the system was solved using a LU decomposition with partial pivoting and row interchanges matrix factorization routine. The latter was taken from the LAPACK library routines available online at [29]. Details about accuracy, computation cost, etc. can be found in [29]. Once the time-averaged temperature distribution is known, it can be substituted in Eqs. (15), (18) and (19) to determine the energy flux distributions along the x and y directions both in the gas and in the plate. Numerical calculations were carried out varying P_A, y_0 and l (half thickness of a plate). The parameters of different runs are listed in Table 1.

4. Results and discussion

The transverse component of the energy flux density at the gas–solid interface ($y = y_0$) for parameters corresponding to run 1 in Table 1 is shown in Fig. 3. These operating conditions where chosen to facilitate the comparison with the test cases of Cao et al. [11] (run 2) and of Ishikawa and Mee [14] (run 7), although the values of the parameters l and K_s have been arbitrarily selected as in these works plate thickness and material have not been modeled (this is further discussed later in this section). Perfectly according to the results obtained by these authors, $\dot{q}_y$ exhibits a sharp peak near the plate extremities letting suppose in these regions a net heat exchange between fluid and solid takes place. In particular, the maximum value of $\dot{q}_y$ is reached when the plate edges are approached: $\dot{q}_{y,\max} = |\dot{q}_y(x=0, y=y_0)| = |\dot{q}_y(x=L_s, y=y_0)|$. This result is further confirmed by the time-averaged temperature distribution illustrated in Fig. 4 for the same run. In the central regions of both the plate and the pore the temperature is nearly uniform over a cross section (isotherms are vertical). As approaching the pore ends, however, the isotherms become closer while their profile results even more curved and practically horizontal at the gas–solid interface. This trend is compatible with a growing transverse temperature gradient $\partial T_m/\partial y$ near the pore ends, so most of the heat transfer between the gas and the plate should be localized in these regions. The monotonic increase of $\dot{q}_y$ at approaching the end section can be interpreted analyzing the cross-sectional distribution of the temperature gradient $\partial T_m/\partial x$ illustrated in Fig. 5 for run 2. As a consequence of the ther-

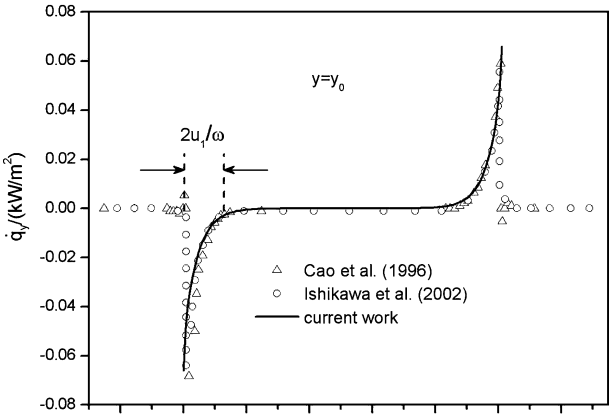

Fig. 3. Time-averaged heat flux density in the y direction at the plate surface ($y = y_0$) as a function of the position along the plate. Solid line is the heat flux density profile computed using the present model (run 1). Open triangles are numerical data from Ref. [11] (run 2). Open circles are numerical data from Ref. [14] (run 7).

Table 1
Parameters of selected simulations

Run	y_0 [m]	l [m]	L_s [m]	x_s [m]	P_A [Pa]	λ [m]	f [Hz]	K_s [W K^{-1} m^{-1}]
1	0.008	0.002	0.25	1.13	170	10.08	100	100
2	0.0047	0.001	0.1	1.8	250	10.08	100	10
3	0.0012–0.0094	0.003	0.25	1.8	200	10.08	100	10
4	0.005	0.003	0.09	1.8	200	10.08	100	10
5	0.00076	0.000095	0.00685	0.04–0.42	2270	1.665	696	5.763
6	0.00055	0.0003	0.07	0.02–0.42	152	1.72	190	0.13

In runs 1–4 test gas is helium at $P_m = 10$ kPa. In run 5 test gas is helium at $P_m = 114.1$ kPa. In run 6 test gas is air at $P_m = 101.325$ kPa. In all cases $T_m = 300$ K.

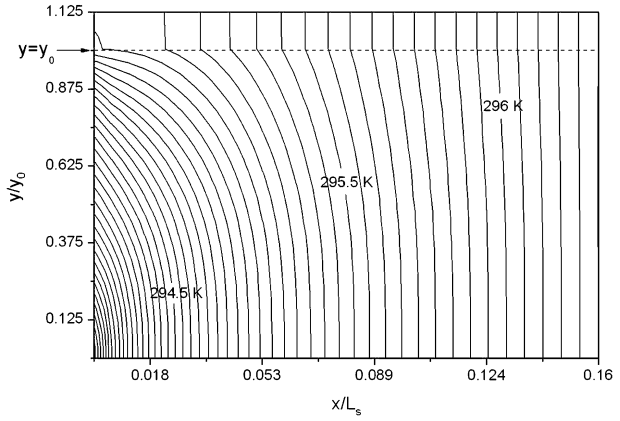

Fig. 4. Time-averaged temperature distribution in half a gas channel and half a solid plate near the left hand edge of the simulated thermally isolated stack for run 1. Temperature of the median isotherm ($x = L_s/2$) has been arbitrarily set to 300 K.

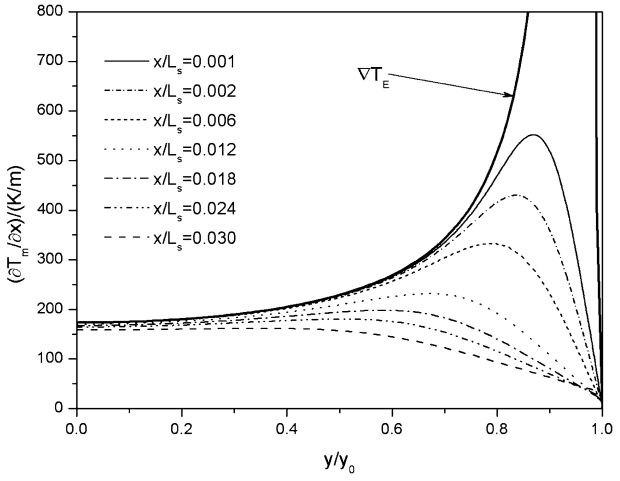

Fig. 5. Transverse distribution (along the y-coordinate) of the longitudinal time-averaged temperature gradient at selected distances from the pore end for run 2. Solid line is a plot of the "end" temperature gradient for which $\dot{h}_x(y) = 0$ deduced from relation (14).

mal isolation boundary condition, in fact, as approaching the pore end ($x/L_s \to 0$) the temperature gradient tends towards the "end" gradient, $\nabla T_E(y)$, for which $\dot{h}_x = 0$. This is a well defined function of the transverse coordinate y which can be determined by equating relation (14) to zero. Energy balance then forces $\dot{q}_y$ to increase continuously to compensate for the decrement of $\dot{h}_x$. It is interesting to observe that near the wall, where the fluid is at rest, $\partial T_m/\partial x$ tends to vanish thus matching the temperature gradient in the plate termination (not shown). In the central regions of the pore, where end effects have no influence, the net heat flux into and out of the plate is zero and the energy transport occurs parallel to the plate along the x direction, as expressed by the standard thermoacoustic theory through relation (14). This is evidenced in Fig. 6 where a good matching is found between numerical (run 3) and analytical results for the axial component of the energy flux density ($\dot{h}_x$) evaluated at the middle of the plate ($x = L_s/2$) for different plate spacing.

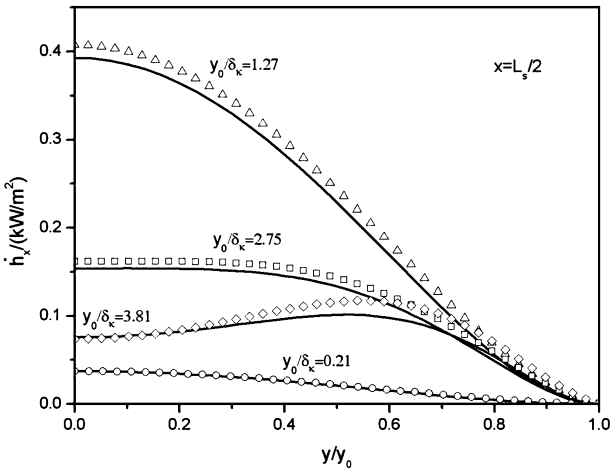

Fig. 6. Transverse distribution (along the y coordinate) of the time-averaged enthalpy flux density in the x direction at the centre of the plate. Solid lines are analytical results of the standard thermoacoustic theory. Points are numerical results of the present model (run 3).

Fig. 3 shows as the distance from the plate end over which a net gas–solid heat transfer takes place is comparable to the peak-to-peak particle displacement amplitude ($2u_1/\omega$); the dependence of this heat-exchange length on acoustic amplitude, plate spacing and Reynolds number has been investigated elsewhere [30].

Numerical simulations performed at different plate thickness, l, reveal that this parameter has no influence on the gas–solid heat-exchange area (if its effect on blockage ratio is not considered): starting from the simulation conditions specified in run 1, the effect of varying l over a factor 10 keeping all the other parameters constant was undetectable. The plate simply serves as a duct which "closes" the energy flux path as imposed by thermal isolation condition.

As expected, the magnitude of the transverse heat flux and the gas–solid heat-exchange area were found to be an increasing function of the plate material thermal conductivity K_s. Smaller the mean temperature gradient in the plate (and in the gas), in fact, greater the axial hydrodynamic energy flux. Anyway, starting from parameter values specified in run 1, the effect of varying K_s by a factor 10^3 keeping all the other parameters constant was of about 1% on $\dot{q}_{y,\max}$ and even less on the gas–solid heat-exchange area. So, run 1 should reproduce at a good level of approximation the simulation conditions of Cao et al. [11] and of Ishikawa and Mee [14].

Since the time-averaged transverse energy flux at the plate surface is positive when entering the plate and negative when leaving the plate, Fig. 3 implies that over the period of an acoustic cycle, energy flows out of the left plate end (close to the nearest velocity antinode), down hydrodynamically along the thermal boundary layer in the gas and into the right plate end (close to the nearest pressure antinode). Being the stack thermally insulated, these energy flows are supplied by the plates themselves, which thus cool at the end which supplies the energy ("cold" end) and heat at the other end which absorbs it ("hot" end). In steady-state, the resulting temperature gradient in the plate gives rise to a diffusive heat flow that perfectly

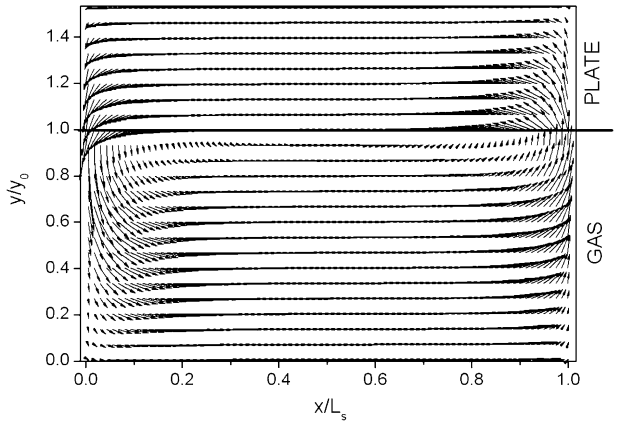

Fig. 7. Time-averaged energy vector pattern for $y_0/\delta_\kappa = 2.1$ and $l/\delta_\kappa = 1.3$ (run 4) in the whole computation domain.

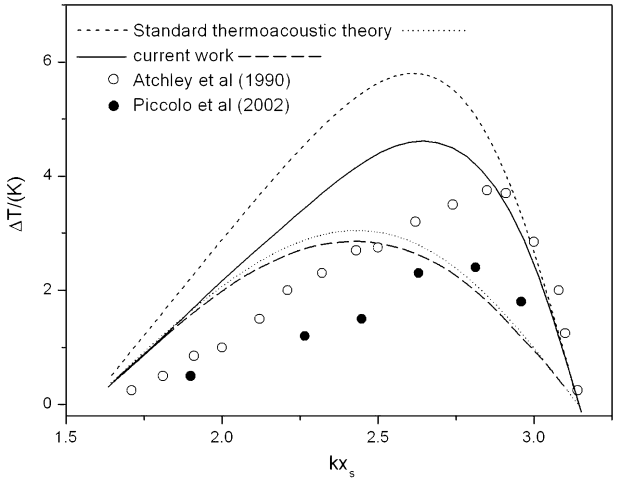

Fig. 8. Time-averaged temperature difference across the stack as a function of stack position in the resonator. Open circles are experimental data Atchley et al. [23]. Full circles are experimental data of Piccolo and Cannistraro [24]. Short-dashed line and continuous line are theoretical predictions respectively of Eq. (28) and of the present model (run 5) to reproduce the data of Atchley et al. Dotted line and dashed line are theoretical predictions respectively of Eq. (28) and of the present model (run 6) to reproduce the data of Piccolo and Cannistraro. Numerical results of the present model are evaluated at the plate centerline ($y = y_0 + l$).

balances the hydrodynamic-one. The overall energy transfer process is clearly displayed for run 4 in Fig. 7 where the time-averaged energy vectors describe a closed "loop".

This picture suggests that an effective model validation can be made by comparing experimental measurements of the steady-state temperature differences across the plates of thermally isolated stacks (ΔT) to the ones numerically computed. In Fig. 8 this comparison is proposed making reference to the experimental data of Atchley et al. [23] and of one of the authors [24]. These data, referring to measurements of the steady state acoustically generated temperature gradients in short parallel-plate stacks without heat exchangers (referred as ThermoAcoustic Couples—TACs) are most suitable for comparison with the present study. In particular, data from Fig. 9 of [23] and from Fig. 4 of [24] have been reproduced here in Fig. 8

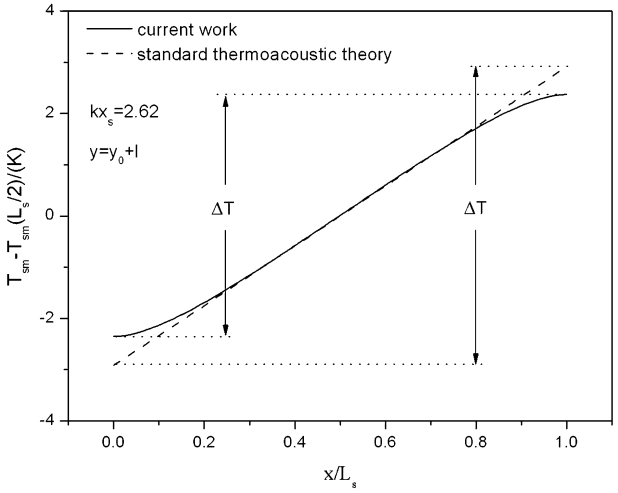

Fig. 9. Centerline time-averaged plate temperature as a function of position along the plate. Solid line is the temperature profile computed using the present model (run 5). Dashed line is the temperature variation predicted by the standard thermoacoustic theory.

(respectively open and full circles) and compared to the numerical computations from this study for runs 5 (solid line) and 6 (dashed line) and to the theoretical predictions of the standard thermoacoustic theory (dotted and short-dashed lines). It should be noted that the temperature differences arising from the numerical computations are taken along the centerline of the plate ($y = y_0 + l$) while those expected from the standard linear theory are directly derived from Eq. (14) by setting a simple energy balance equation. This last is easily obtained observing that in the standard linear theory T_m is assumed y-independent so the total enthalpy flux in half a channel is:

$$\dot{H} = \int_0^{y_0} \dot{h}_x(y)\,\mathrm{d}y = \dot{H}_\alpha - \frac{\mathrm{d}T_m}{\mathrm{d}x}\dot{H}_\beta \tag{25}$$

where

$$\dot{H}_\alpha = \int_0^{y_0} \dot{h}_\alpha(y)\,\mathrm{d}y, \qquad \dot{H}_\beta = \int_0^{y_0} \dot{h}_\beta(y)\,\mathrm{d}y \tag{26}$$

In steady-state this hydrodynamic energy flow must be balanced by a diffusive-one flowing in the opposite direction both in the gas and in the plate:

$$\left(\dot{H}_\alpha - \frac{\mathrm{d}T_m}{\mathrm{d}x}\dot{H}_\beta\right) - \left(K y_0 \frac{\mathrm{d}T_m}{\mathrm{d}x} + K_s l \frac{\mathrm{d}T_{sm}}{\mathrm{d}x}\right) = 0 \tag{27}$$

Observing now that $\mathrm{d}T_m/\mathrm{d}x = \mathrm{d}T_{sm}/\mathrm{d}x$ and replacing $\mathrm{d}T_m/\mathrm{d}x$ with $\Delta T/\Delta x$ ($\mathrm{d}T_m/\mathrm{d}x$ is prescribed as constant by the standard linear theory) the following formula is found for the temperature difference expected between the plate extremities:

$$\Delta T = \frac{\dot{H}_\alpha L_s}{K y_0 + K_S l + \dot{H}_\beta} \tag{28}$$

Fig. 8 shows that the deviation between the experimental data and the theoretical predictions of (28) is of about 172% for the data of Atchley et al. and of about 109% for the other case. These deviations decrease respectively to 94 and 99% if the

simplified two-dimensional model proposed in the present work is employed. The improved matching can be explained by examination of Fig. 9 where the mean temperature along the centerline of the solid plate obtained by the present model for run 5 (continuous line) is plotted as a function of the plate length with the stack held fixed at location $kx_s = 2.62$ (almost midway between pressure node and antinode). Also shown (dashed line) is the temperature profile predicted by the standard theory through Eq. (28). In the middle of the plate the centerline plate temperature exhibits essentially a linear profile which closely overlaps the one predicted by the standard theory. Approaching the plate ends, however, the temperature profile results slightly curved and gives rise to a smaller temperature difference ΔT than that arising from a constant temperature gradient over the whole plate length. These curvatures are an evidence of the temperature stratification which originates near the ends of the plate and which constitutes the driving force for the transverse heat fluxes entering and leaving the plate near its edges. As the proposed computation methodology relies on the standard linear thermoacoustic theory (no extension or refinement is made) this result suggests that the deviations found between linear theory predictions and experimental data at low and moderate acoustic Mach numbers, are not entirely due to non-linear effects but that thermal effect localized at the stack edges may also play an important role. Similar trends were observed by Worlikar et al. [13] and, more recently, by Marx and Blanc-Bennon [31].

Finally, we report some observations on the results obtained at high Mach numbers, when temperature gradients become relevant. At sufficiently high acoustic pressures we observe in the gas the appearance of regions where the direction of the energy flow is reversed (from the "hot" to the "cold" end). This result is not surprising and corresponds to the well-known fact that, in dependence of the value of the mean axial temperature gradient, a stack can be operated in the heat pump or in the prime mover mode. In the inviscid case, the boundary between the two operation regimes is clearly defined by the "critical" temperature gradient [1] but, in the presence of viscosity, the boundary is less marked. In our case the effect is evident where $\partial T_m/\partial x$ is over the local value of $\nabla T_E(y)$.

5. Conclusions

The essential features of the time-averaged temperature and heat flux density distributions near the edges of a thermally isolated thermoacoustic stack are investigated through a simple numerical calculus-scheme based on the classical linear thermoacoustic theory. The simulation results agree well with those of other numerical computations available in literature. A net heat exchange between the oscillating gas and the solid wall occurs only near the stack edges at a distance from the ends not exceeding the peak-to-peak particle displacement amplitude. The non-uniformity of the distribution of the temperature gradient at the plate ends is the main result presented here. This thermal effect may play an important role as source of the deviations generally found between linear theory predictions and experimental data at low and moderate Mach numbers.

In its current form, the model is expected to be valid when restricted to situations where the classical solution for the amplitude of the temperature oscillations T_1 may be retained accurate near the pore terminations. This should be reasonably verified when transverse temperature gradients are weak, namely when stacks are operated at low Mach number. This conclusion is further enforced observing that the model, being based on the equations of the standard linear theory, does not take into account for non-linear effects (presence of harmonics greater than the fundamental) or turbulent oscillatory flow, vortex generation, jetting (which can become relevant near the stack edges). These effects could generate transverse heat fluxes greater than the ones obtained uniquely by thermal conduction so the other key hypothesis on which the present model is based may be invalidated.

References

[1] G.-W. Swift, Thermoacoustic engines, J. Acoust. Soc. Amer. 84 (1988) 1145–1180.
[2] M.-E.-H. Tijani, J.-C.-H. Zeegers, A.-T.-A.-M. de Waele, The optimal stack spacing for thermoacoustic refrigeration, J. Acoust. Soc. Amer. 112 (2002) 128–133.
[3] M.-E.-H. Tijani, J.-C.-H. Zeegers, A.-T.-A.-M. de Waele, Design of thermoacoustic refrigerators, Cryogenics 42 (2002) 49–57.
[4] G.-W. Swift, Analysis and performance of a large thermoacoustic engine, J. Acoust. Soc. Amer. 92 (1992) 1551–1563.
[5] S. Duffourd, Refrigérateur thermoacoustique: etudes analytiques et expérimentales en vue d'une miniaturization, PhD thesis, Ecole Centrale de Lyon, 2001.
[6] Ph. Blanc-Bennon, High amplitude effects in thermoacoustic refrigerators, in: O.V. Rudenko, O.A. Sapozhnikov (Eds.), Proceedings of 16th International Symposium on Nonlinear Acoustics (ISNA) in Nonlinear Acoustics at the Beginning of the 21st Century, vol. 1, Moscow State University, Moscow, Russia, 2002, pp. 171–178.
[7] M. Wetzel, C. Herman, Accurate measurement of high-speed, unsteady temperature fields by holographic interferometry in the presence of periodic pressure variations, Measurement Sci. Technol. 9 (1998) 939–951.
[8] W.-P. Arnott, H.-E. Bass, R. Raspet, General formulation of thermoacoustics for stacks having arbitrarily shaped pore cross sections, J. Acoust. Soc. Amer. 90 (1991) 3228–3237.
[9] G.-W. Swift, R.-M. Keolian, Thermoacoustics in pin-array stacks, J. Acoust. Soc. Amer. 94 (1993) 941–943.
[10] J.A. Adeff, T.-J. Hofler, A.-A. Atchley, W.-C. Moss, Measurements with reticulated vitreous carbon stacks in thermoacoustic prime movers and refrigerators, J. Acoust. Soc. Amer. 104 (1998) 32–38.
[11] N. Cao, J.-R. Olson, G.-W. Swift, S. Chen, Energy flux density in a thermoacoustic couple, J. Acoust. Soc. Amer. 99 (1996) 3456–3464.
[12] A.-S. Worlikar, O.-M. Knio, Numerical simulation of a thermoacoustic refrigerator I. Unsteady adiabatic flow around the stack, J. Comput. Phys. 127 (1996) 424–451.
[13] A.-S. Worlikar, O.-M. Knio, R. Klein, Numerical simulation of a thermoacoustic refrigerator II. Stratified flow around the stack, J. Comput. Phys. 144 (1998) 299–324.
[14] H. Ishikawa, D.-J. Mee, Numerical investigations of flow and energy fields near a thermoacoustic couple, J. Acoust. Soc. Amer. 111 (2002) 831–839.
[15] E. Besnoin, O.-M. Knio, Numerical study of thermoacoustic heat exchangers in the thin plate limit, Numer. Heat Transfer A 40 (2001) 445–471.
[16] D. Marx, Ph. Blanc-Bennon, Numerical simulation of stack–heat exchangers coupling in a thermoacoustic refrigerator, AIAA J. 42 (2004) 1338–1347.
[17] G. Mozurkewich, Time average temperature distribution in a thermoacoustic stack, J. Acoust. Soc. Amer. 103 (1998) 380–388.
[18] G. Mozurkewich, A model for transverse heat transfer in thermoacoustic, J. Acoust. Soc. Amer. 103 (1998) 3318–3326.

[19] A. Gopinath, N.-L. Tait, S.-L. Garrett, Thermoacoustic streaming in a resonant channel: The time-averaged temperature distribution, J. Acoust. Soc. Amer. 103 (1998) 1388–1405.
[20] V. Gusev, P. Lotton, H. Bailliet, S. Job, M. Bruneau, Relaxation-time approximation for analytical evaluation of temperature field in thermoacoustic stack, J. Sound Vib. 235 (2000) 711–726.
[21] V. Gusev, P. Lotton, H. Bailliet, S. Job, M. Bruneau, Thermal wave harmonics generation in the hydrodynamical heat transport in thermoacoustics, J. Acoust. Soc. Amer. 109 (2001) 84–90.
[22] R. Waxler, Stationary velocity and pressure gradients in a thermoacoustic stack, J. Acoust. Soc. Amer. 109 (2001) 2739–2750.
[23] T.-J. Atchley, A.-A. Hofler, M.-L. Muzzerall, M.-D. Kite, C. Ao, Acoustically generated temperature gradients in short plates, J. Acoust. Soc. Amer. 88 (1990) 251–263.
[24] A. Piccolo, G. Cannistraro, Convective heat transport along a thermoacoustic couple in the transient regime, Int. J. Thermal Sci. 41 (2002) 1067–1075.
[25] L.D. Landau, E.M. Lifshitz, Fluid Mechanics, first ed., Pergamon, London, 1959, p. 184.
[26] G.W. Swift, Thermoacoustics: A Unifying Perspective for Some Engines and Refrigerators, Acoustical Society of America, 2002.
[27] G.-W. Swift, A. Migliori, T. Hofler, J. Wheatley, G.-W. Swift, Theory and calculations for an intrinsically irreversible acoustic prime mover using liquid sodium as primary working fluid, J. Acoust. Soc. Amer. 78 (1985) 767–781.
[28] A.-O. Santillan, R.-R. Bullosa, Space dependence of acoustic power and heat flux in the thermoacoustic effect, Int. Comm. Heat Mass Transfer 22 (1995) 539–548.
[29] http://www.netlib.org/lapack.
[30] A. Piccolo, G. Pistone, Estimation of heat transfer coefficients in oscillating flows: the thermoacoustic case, Int. J. Heat Mass Transfer 49 (2006) 1631–1642.
[31] D. Marx, Ph. Blanc-Bennon, Numerical calculation of the temperature difference between the extremities of a thermoacoustic stack plate, Cryogenics 45 (2005) 163–172.